

# Relationship Between ACSL4-Mediated Ferroptosis and Chronic Obstructive Pulmonary Disease

Yingxi Wang<sup>1</sup>, Shuyue Xia<sup>2</sup> 

<sup>1</sup>Graduate School, Dalian Medical University, Dalian, Liaoning, People's Republic of China; <sup>2</sup>Department of Respiratory and Critical Care Medicine, Central Hospital Affiliated to Shenyang Medical College, Shenyang, Liaoning, People's Republic of China

Correspondence: Shuyue Xia, Department of Respiratory and Critical Care Medicine, Central Hospital Affiliated to Shenyang Medical College, Shenyang, Liaoning, 110075, People's Republic of China, Tel/Fax +86-24-85715588, Email syx262@126.com

**Purpose:** Although cigarette smoke exposure is the major risk factor for chronic obstructive pulmonary disease (COPD), the mechanism is not completely understood. The aim of the present study was to investigate whether ACSL4-mediated ferroptosis in lung epithelial cells plays a part in the COPD development process and its association.

**Patients and Methods:** In this study, animal and cell models of COPD were modelled using cigarette smoke extracts (CSEs), and cell viability, lipid ROS, iron ion deposition, and ferroptosis-related markers were measured in lung tissue and lung epithelial cells following CSE exposure. Morphological changes in mitochondria were observed in lung tissue and epithelial cells of the lung by transmission electron microscope. The expression levels of ACSL4 mRNA and protein in lung tissue and epithelial cells were measured by real-time PCR and Western blotting. In addition, animal-interfering lentivirus and cell-interfering RNA against ACSL4 were constructed in this study, ferroptosis in lung tissue and lung epithelial cells after ACSL4 interference was detected, and ACSL4 mRNA and protein expression levels were detected.

**Results:** CSE induced ferroptosis in lung tissues and lung epithelial cells, and the expression levels of ACSL4 were elevated in CSE-treated lung tissues and lung epithelial cells. After ACSL4 interference, the expression of ACSL4 decreased, mitochondrial morphology was restored, and ferroptosis in lung tissues and lung epithelial cells was alleviated. Both respiratory frequency and enhanced pause of COPD mice models decreased after ACSL4 interference.

**Conclusion:** ACSL4-mediated ferroptosis in lung epithelial cells is associated with COPD and positively correlated with ferroptosis in epithelial cells.

**Keywords:** ACSL4, ferroptosis, chronic obstructive pulmonary disease

## Introduction

Chronic obstructive pulmonary disease (COPD) is a common and frequently recurring disease in clinical practice, mainly characterized by a slow decline in lung function and progressive airflow limitation, which is not completely reversible and severely affects the ability of patients to work and their quality of life and creates a tremendous social and economic burden.<sup>1,2</sup> Cigarette smoke is the main risk factor for COPD, but the mechanism of smoke-mediated COPD is not fully understood and needs to be further elucidated. One of the major pathological changes in COPD is damage to the pulmonary epithelial tissue, and its regulatory mechanism is complex. The major pathways recognized in COPD pathology are mainly associated with airway inflammation, oxidative stress and protease-antiprotease imbalance. Nevertheless, in recent years, some studies have presented new ideas. When iron-oxide nanoparticles were given to rats, free radicals were significantly enhanced and glutathione was significantly reduced, while histological findings showed that the nanoparticles caused emphysema, mesenchymal congestion and lung inflammation in rats, confirming the toxic effects of iron nanoparticles on lung tissue.<sup>3</sup>

Cell ferroptosis is a novel cell death pattern characterized by the accumulation of iron-dependent lipid peroxides and has been shown to be involved in pathophysiologic processes in many diseases.<sup>4</sup> CS mediates ferroptosis in epithelial cells and promotes the development of COPD.<sup>5</sup> However, the correlation between ferroptosis and COPD remains unclear and needs to be further investigated.

Acyl-CoA synthetase long-chain family member 4 (ACSL4) can promote the production of phosphatidylethanolamine (PE) from arachidonic acid (AA) and adrenaline, which is closely related to ferroptosis.<sup>6,7</sup> Various studies have shown that ACSL4 can mediate ferroptosis and participate in the occurrence and development of various diseases, but the role and mechanism of ACSL4 in COPD have not been reported.<sup>8–10</sup> Using KEGG analysis, it was found that ACSL4 is closely related to ferroptosis. In addition, researchers downloading analysis of raw chip experimental data (GSE18344) from the GEO database found that ACSL4 was aberrantly elevated in the lung tissue of mice exposed to cigarette smoke,<sup>11</sup> while a proteintlas database search revealed ACSL4 expression in human lung epithelial cells. Therefore, ACSL4 is likely to participate in the development of COPD by mediating ferroptosis of lung epithelial cells. In the present study, ferroptosis in COPD induced by cigarette smoke was validated at both the animal and cellular levels, and whether ACSL4 mediates ferroptosis in COPD lung epithelial cells was investigated by constructing interference lentiviruses and siRNAs to provide a new direction for the pathogenesis of COPD and a new idea for the targeted treatment of COPD.

## Materials and Methods

### Cigarette Smoke Extract (CSE) Preparation

As previously reported,<sup>12</sup> five cigarettes (tar: 11mg; nicotine 1mg; carbon monoxide 11mg) (Liquan, Zhejiang China Tobacco Industry Co., Ltd., China) were burned and collected in containers containing 10 mL PBS to dissolve as much output as possible. The pH was adjusted to 7.2–7.4, and the solution was then filtered using a filter of 0.22  $\mu\text{m}$  for experimental purposes. CSE was prepared before each experiment to ensure that the CSE used was fresh.

### Animal Models

Six-week-old male BALB/c mice of Specific Pathogen Free (SPF) grade were selected and weighed 21–23 g (Liaoning Changsheng Biotechnology co., Ltd., Benxi, Liaoning, China). After a week of adaptive feeding, the mice were randomly assigned to four groups (Control, CSE, CSE+LV-shNC, CSE+LV-shACSL4), each consisting of 6 animals. Mice in the control group received 0.3 mL of PBS intraperitoneally on Days 0, 11, and 22, while mice in the remaining three groups received 0.3 mL of CSE intraperitoneally on Days 0, 11, and 22. Mice in the CSE+LV-shNC and CSE+LV-shACSL4 groups received intratracheal infusions of Lentiviral vector containing unrelated sequence (LV-shNC) (Fenghbio, BR004, Changsha, Hunan, China) and Lentiviral vector containing ACSL4 (LV-shACSL4) ( $10^8$  TU/mL) (Fenghbio, BR004, Changsha, Hunan, China) on Day 14, respectively, while mice in the control and CSE groups received intratracheal transfusions of an equal volume of PBS on Day 14.<sup>12,13</sup> Each group of mice was sacrificed on Day 28, and lung tissue was collected for follow-up assessments. Before being sacrificed on Day 28, the respiratory frequency (f) and the enhanced pause (Penh) of the mice in each group were detected with a non-invasive pulmonary function testing system for small animals (analog interface-16, Emka, France). With the approval of the Ethics Committee of Central Hospital affiliated to Shenyang Medical College, the study was conducted in accordance with the Guide for the Care and Use of Laboratory Animals of the National Institutes of Health.

### Haematoxylin-Eosin (H&E) Staining

Lung tissue from COPD mice was immobilized overnight in 4% paraformaldehyde, dehydrated in ethanol and embedded in paraffin. Sample wax cubes were cut into 5  $\mu\text{m}$  slices and dyed with haematoxylin (Solarbio, H8070, Beijing, China) and eosin (Sangon, A600190, Shanghai, China). The sections were observed and photographed under a microscope. The mean linear intercept (MLI) and destructiveness index (DI) were measured to assess emphysema.<sup>12,13</sup>

## Prussian Blue Staining

Prussian blue staining (Servicebio, G1029, Wuhan, Hubei, China) was used to observe iron deposition in lung tissue. Prussian blue staining solution was added dropwise to the prepared lung tissue sections for 1 hour. After rinsing in distilled water, Prussian blue staining solution was added and stained for 3 minutes. Finally, the slices were washed with water until the running water was colourless, dehydrated with anhydrous ethanol, and neutral gum was added to seal the slices. The staining effect was observed under a microscope and photographed.

## Cell Culture and Intervention

Normal human bronchial epithelial BEAS-2B cells (iCell, iCell-h023, Shanghai, China) were cultured in DMEM (Servicebio, G4510, Wuhan, Hubei, China) containing 10% foetal bovine serum (Evergreen, 11011-8611, Hangzhou, Zhejiang, China) in an incubator based at 37 °C and 5% CO<sub>2</sub>.

(1) BEAS-2B cells were randomized into 5 groups. The CSE intervention groups were treated with 5% CSE for 24 hours. The CSE+Fer-1 groups were co-intervened with 5% CSE and 1 μM, 5 μM, and 10 μM Ferrostatin-1 (Fer-1) (Yuanye Bio, S81461, Shanghai, China) for 24 hours respectively. Finally, the control group was not given any treatment. The best Fer-1 concentration was selected for subsequent experiments in this section.

(2) Log-stage BEAS-2B cells were transfected with ACSL4 siRNA (General Biol, Anhui, China) or NC (General Biol, Anhui, China) for 48 hours and divided into five groups, siNC, siNC+CSE, siACSL4, siACSL4+CSE, and siACSL4+CSE+Fer-1, and all cells were collected at the same time 24 hours after co-intervened with 5% CSE or 5% CSE+ 5 μM Fer-1.<sup>5</sup>

## Cell Viability Assay

The cells were inoculated in 96-well culture plates with 3×10<sup>3</sup> cells per hole. After the treatment conditions were completed, Cell Counting Kit-8 (CCK-8) (Wanleibio, WLA074, Shenyang, China) was added, and the cells were placed in incubators at 37 °C and 5% CO<sub>2</sub>, for 2 hours. The OD was determined at 450 nm.

## Detection of Iron Ion Content

One millilitre of detection buffer was used to resuspend cells, which were then homogenized in an ice bath and centrifuged at 16,000 × g for 10 min at 4°C, after which the supernatant was collected, and an iron detection kit (abcam, Ab83366, Shanghai, China) was used to detect the iron ion content. The standard concentration was the ordinate, the calibrated OD value was the abscissa, and the corresponding concentration was calculated according to the standard curve.

## Streaming Lipid ROS Detection

Cells were cultured in 6-well plates, treated as described above, and assayed after reaching the time point. C11-BODIPY581/591 (2 μM) (Maokangbio, MX5211, Shanghai, China) was added to the cells after the treatment conditions were completed and incubated for 20 min. The cells were washed twice with PBS and collected. After the cells were resuspended, flow cytometry was performed.

## Detection of Ferroptosis-Related Markers

The cell suspension or the supernatant of the tissue homogenate was taken for assay. A protein standard curve was prepared using a BCA protein concentration assay kit (Wanleibio, WLA004, Shenyang, China), the protein concentration in each sample was calculated using a standard curve, and the protein concentrations were standardized. Superoxide dismutase (SOD), malondialdehyde (MDA) and glutathione (GSH) levels were measured using superoxide dismutase (Wanleibio, WLA110, Shenyang, China), malondialdehyde (Wanleibio, WLA048, Shenyang, China), and reduced glutathione kits (Wanleibio, WLA105, Shenyang, China).

## Real-Time PCR

Total RNA was extracted from tissues or cells using TRIzol (BioTeke, RP1001, Beijing, China), and the resulting RNA samples were reverse transcribed using BeyoRT II M-MLV (BeyoTime, D7160L, Shanghai, China) reverse transcriptase

**Table 1** List of Genetic Primers

Name	Sequence (5'-3')
mus ACSL4 F	AGAAGGATCTTGGGTGA
mus ACSL4 R	GCTTGAAGGCATCTGTTA
mus $\beta$ -actin F	CTGTGCCCATCTACGAGGGCTAT
mus $\beta$ -actin R	TTTGATGTACGCACGATTTCC
homo ACSL4 F	GCATTCCTCCAAGTAGACC
homo ACSL4 R	ATGAGCCAAAGGCAAGT
homo $\beta$ -actin F	GGCACCCAGCACAATGAA
homo $\beta$ -actin R	TAGAAGCATTTGCGGTGG

**Table 2** Interference and Negative Control Sequence

Name	Sequence (5'-3')
siNC	UUCUCCGAACGUGUCACGUTT ACGUGACACGUUCGGAGAATT
siACSL4-1	GUAUGUAUCUCUUGGGAAATT UUUCCCAAGAGAUACAUAUACTT
siACSL4-2	CGGAAAUCAUGGAUAGAAUTT AUUCUAUCCAUGAUUUCCGTT
siACSL4-3	GCAAAGAAGCAGUAGUUCATT UGAACUACUGCUUCUUUGCTT

to produce the corresponding cDNA. Real-time PCR analysis was performed on an Exicycler 96 instrument (Bioneer Corporation, Daejeon, Korea) using a SYBR Green PCR Kit (Solarbio, SY1020, Beijing, China). The relative expression of mRNAs was normalized to  $\beta$ -actin. The primer sequences are shown in Table 1. Interference sequences and negative control sequences are shown in Table 2.

## Western Blot Analysis

Total proteins were extracted from tissues or cells using a lysis buffer (Wanleibio, WLA019, Shenyang, China). Proteins were quantified using a BCA protein assay kit (Wanleibio, WLA004, Shenyang, China). The denatured proteins are then separated by SDS-PAGE followed by an electrophoretic transfer onto a PVDF membrane. After blocking with 5% nonfat dry milk at room temperature for an hour, the membranes were incubated with the primary antibodies against ACSL4 (Abclonal, A6826, Wuhan, Hubei, China), glutathione peroxidase 4 (GPX4) (Abclonal, A11243, Wuhan, Hubei, China) and ferritin heavy chain (FTH) (Wanleibio, WL05360, Shenyang, China) at 4 °C. The membranes were then incubated with diluted secondary antibodies (1:5000, Wanleibio, WLA023, Shenyang, China). Quantification of band intensities was performed using Gel-Pro-Analyser software.

## Transmission Electron Microscopy

Cells or tissue samples were collected, fixed in 1% osmic acid at room temperature in the dark for 2 hours, dehydrated with acetone, and polymerized in a 60 °C oven for 48 hours. Specimens were sliced into 60–80 nm ultrathin sections and stained with 2% saturated uranyl acetate alcohol solution and 2.6% lead citrate solution, followed by observation of mitochondrial morphology changes under a transmission electron microscope (HT-7700, Hitachi, Japan).

## Statistical Analysis

All data in this study were statistically analysed using SPSS 25.0. All study data were normalized and expressed as the mean  $\pm$  standard deviation. Data distribution was validated using the Shapiro–Wilk test. Single-factor ANOVA was used for multigroup comparisons.  $P < 0.05$  was considered statistically significant for data analysis.

## Results

### High Expression of ACSL4 in the Lung Tissue of COPD Mice

In this study, a COPD mouse model was constructed. ACSL4 mRNA and protein expression levels were significantly increased in CSE mouse lung tissue compared to controls. Compared with the CSE or CSE+LV-shNC group, the mRNA and protein levels of ACSL4 in mouse lung tissue from the CSE+LV-shACSL4 group were significantly downregulated (Figure 1A and B). COPD is mainly caused by the destruction of alveolar walls and the thinning of alveolar sacs due to persistent chronic inflammation.<sup>1</sup> The normal control group showed clear alveolar structures and relatively regular arrangement; enlarged alveoli spaces were detected in the CSE groups, as shown by HE staining, along with rupture of the alveolar septa and fusion of the alveoli, along with emphysema (Figure 1E), high DI and MLI (Figure 1C and D). Compared with the CSE+LV-shNC group, the lung injury of the CSE+LV-shACSL4 group was significantly alleviated, and the DI and MLI were also significantly decreased. Only mild alveolar space enlargement and pulmonary septum fracture were observed in the lung tissue of the CSE+LV-shACSL4 group, emphysema was significantly improved (Figure 1E), and DI and MLI were significantly reduced (Figure 1C and D). The lung function results of the mice showed that compared with the normal control group, the respiratory frequency and the enhanced pause of the CSE group were significantly increased ( $P < 0.05$ ). Compared with CSE or CSE+LV-shNC group, the respiratory frequency and the enhanced pause of CSE+LV-shACSL4 group were significantly decreased ( $P < 0.05$ ). The lung function results are shown in Table 3.

### ACSL4 Induces Ferroptosis in Lung Tissue of COPD Mice

To detect ferroptosis in the lung tissue of COPD mice, ferroptosis-related markers were evaluated in the lung tissue of mice in each group. Compared to the control, the contents of SOD and GSH in the lung tissue of CSE mice were significantly decreased, and the MDA content was significantly increased. Compared with the CSE or the CSE+LV-shNC group, the contents of SOD and GSH were significantly increased in the CSE+LV-shACSL4 group, and MDA was significantly decreased (Figure 2A–C).

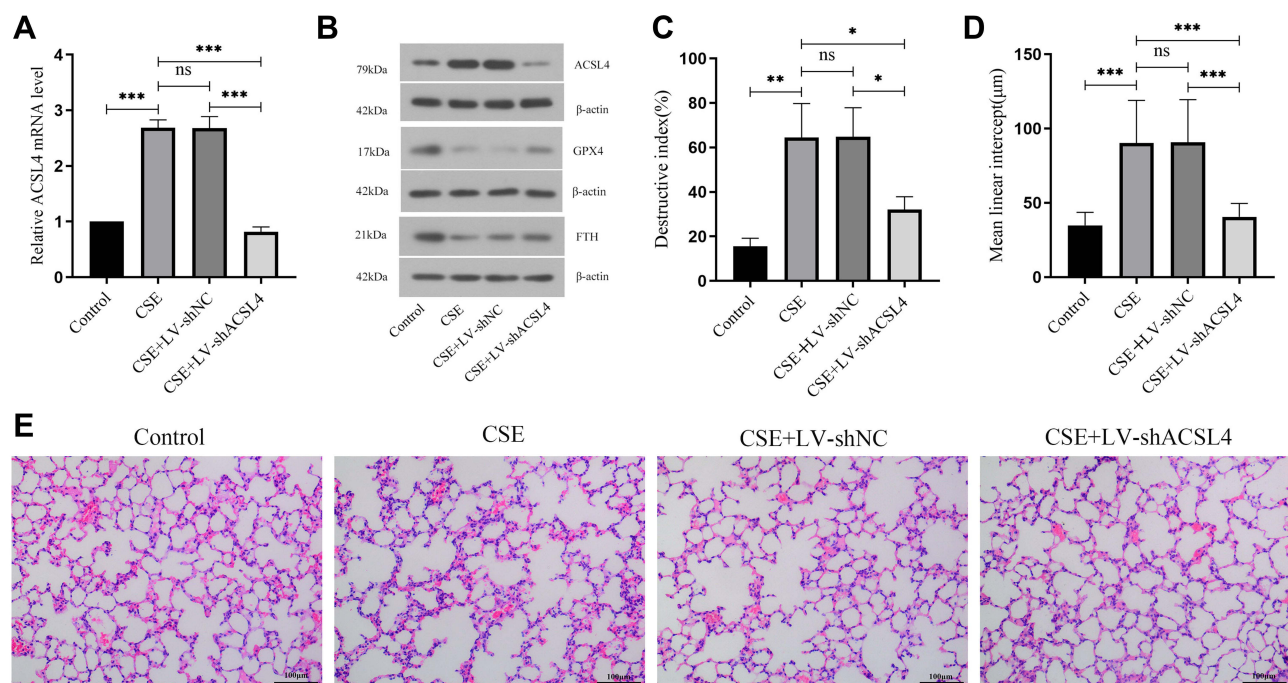


**Figure 1** ACSL4 is highly expressed in the lung tissue of COPD mice. **(A)** Relative expression of ACSL4 mRNA in mouse lung tissue by real-time PCR. **(B)** The expression of ACSL4 protein and ferroptosis-related proteins GPX4 and FTH in COPD mouse lung tissue was detected by Western blotting. **(C–E)** HE staining of sections of mouse lung tissue. The DI and MLI values of each group were calculated. Data are presented as the mean  $\pm$  SD of three replicates and analyzed using one-way ANOVA followed by post-hoc multiple comparisons. (<sup>ns</sup> $p > 0.05$ , \* $p < 0.05$ , \*\* $p < 0.01$ , \*\*\* $p < 0.001$ ).

**Table 3** Lung Function

Parameters	Control	CSE	CSE+LV-shNC	CSE+LV-shACSL4
f (breaths/min)	378.954±51.758	538.656±60.068 <sup>a</sup>	540.978±46.852	398.342±94.812 <sup>bc</sup>
P (mL/sec)	0.532±0.027	0.736±0.081 <sup>a</sup>	0.788±0.125	0.56±0.047 <sup>bc</sup>

**Notes:** <sup>a</sup>p<0.05, in comparison to the control group. <sup>b</sup>p<0.05, in comparison to the CSE group. <sup>c</sup>p<0.05, in comparison to the CSE+LV-shNC group.

Iron deposits in lung tissue were then observed by Prussian blue staining. In the normal control group, there was no obvious deposition of iron ions in lung tissues, while the deposition of iron ions in lung tissue of the CSE and CSE+LV-shNC group mice was significantly increased, and the iron ion deposition in CSE+LV-shACSL4 mouse lung tissue was significantly decreased (Figure 2D).

The morphological changes in mitochondria in lung tissue were observed by transmission electron microscopy. The mitochondria in the lung tissue of the normal control group were intact, double-membrane-coated, “kidney-type” structures, with clearly visible cristae. In CSE and CSE+LV-shNC mice, the mitochondrial morphology of lung tissue was altered, wrinkled, fractured into cristae, and vacuolated. The degree of damage to CSE+LV-shACSL4 mitochondria

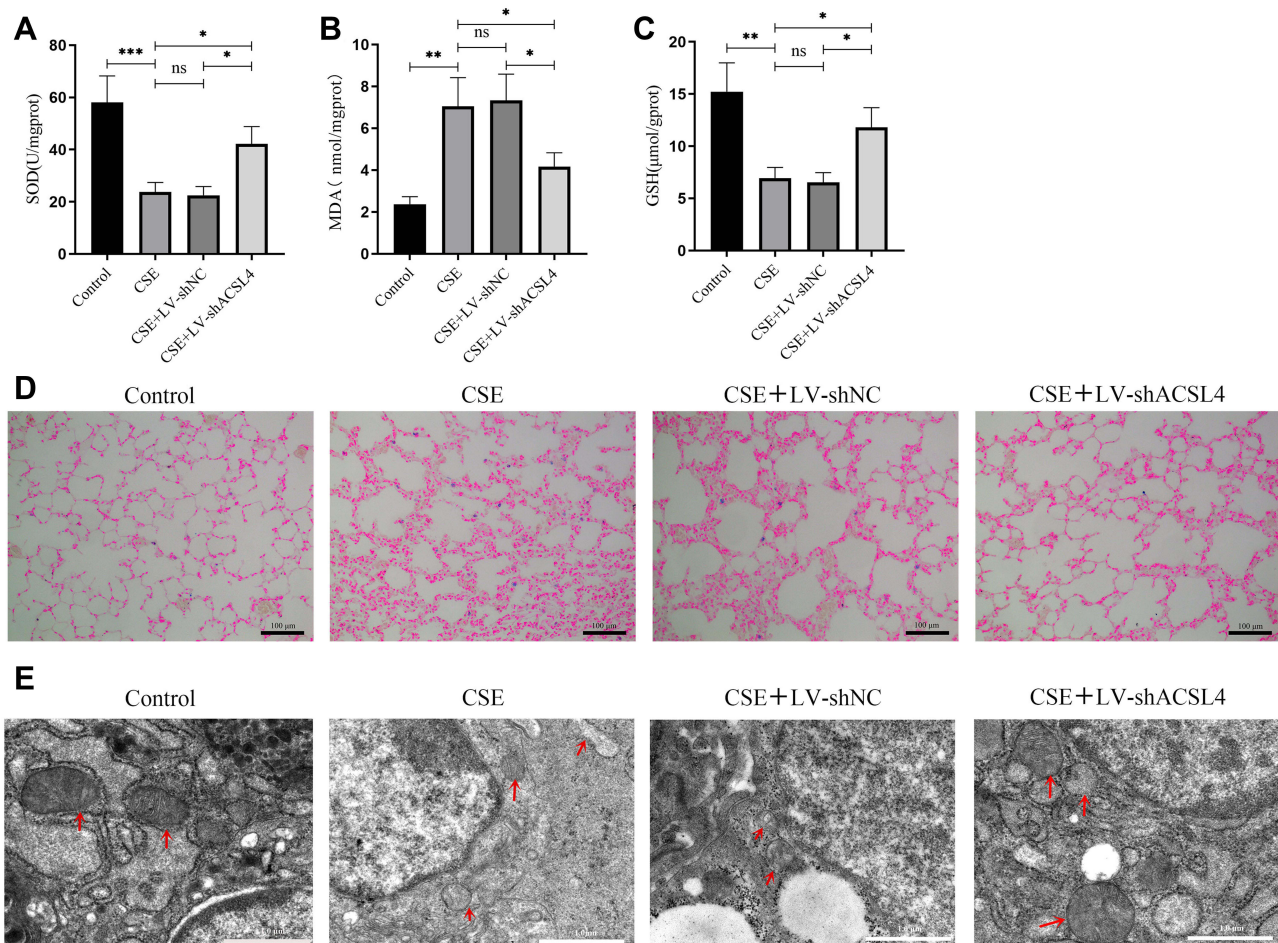


**Figure 2** ACSL4 induces ferroptosis in lung tissue of COPD mice. (A–C) Lung tissue from each group of mice was analysed for markers related to ferroptosis. (D) Iron deposition in lung tissue from mice in each group was observed by Prussian blue staining. (E) Transmission electron microscopy revealed the mitochondrial morphology in lung tissue from mice in each group; red arrows indicate mitochondria. Data are presented as the mean ± SD of three replicates and analyzed using one-way ANOVA followed by post-hoc multiple comparisons. (<sup>ns</sup>p > 0.05, \*p < 0.05, \*\*p < 0.01, \*\*\*p < 0.001).

was reduced; even though vacuolated mitochondria were observed, most of the mitochondrial cristae were arranged in an orderly manner and clearly visible (Figure 2E).

## ACSL4 Induces Ferroptosis in COPD Lung Epithelial Cells

BEAS-2B cells were treated with CSE to construct a COPD cell model. The first step was to use CCK-8 to detect cell viability in each group. Cell viability was significantly reduced in the CSE group compared to the control group. After administration of different concentrations of Fer-1 (1  $\mu$ M, 5  $\mu$ M, 10  $\mu$ M), cell viability increased with Fer-1 concentration compared to the CSE group (Figure 3A). Here, the optimal concentration of Fer-1 was screened at 5  $\mu$ M for subsequent experiments.

To verify the occurrence of ferroptosis in BEAS-2B cells of COPD induced by CSE, this study examined the deposition of iron ions in lung epithelial cells. There was a significant increase in iron ion content in the CSE group compared to the control. After treatment with different concentrations of Fer-1 (1  $\mu$ M, 5  $\mu$ M, 10  $\mu$ M), the iron ion content decreased with the Fer-1 concentration compared to that in the CSE group (Figure 3B).

Then, lipid peroxidation during ferroptosis was detected, and the content of lipid ROS in cells was detected by flow cytometry. There was a strong increase in lipid ROS content in the CSE group compared to the control. After different concentrations of Fer-1 (1  $\mu$ M, 5  $\mu$ M and 10  $\mu$ M) were administered, the content of lipid ROS decreased gradually with increasing concentrations of Fer-1 compared to the CSE group (Figure 3C).

Finally, the level of ACSL4 expression in BEAS-2B cells was detected by real-time PCR and Western blotting. Compared to the control group, the mRNA and protein expression levels of ACSL4 in the CSE group increased significantly. The mRNA and protein expression levels of ACSL4 decreased with Fer-1 concentration compared to the CSE group after administration of different concentrations of Fer-1 (Figure 3D–E).

In addition, to verify the ferroptosis of lung epithelial cells after interfering with ACSL4, we constructed 3 siRNAs against human ACSL4 and control NC and transferred them into BEAS-2B cells. Compared to the NC group, the siACSL4-1, siACSL4-2, and siACSL4-3 groups had significantly lower ACSL4 mRNA and protein expression levels. Among them, the siACSL4-2 group had the highest interference efficiency and was used for subsequent experiments (Figure 3F–G).

## Interference with ACSL4 Can Alleviate Ferroptosis of Lung Epithelial Cells

The optimal concentrations of Fer-1 and siACSL4 with the best interference efficiency were chosen to jointly intervene with BEAS-2B to verify the effect of ACSL4 on pulmonary epithelial cell ferroptosis, as mentioned above. First, the mRNA expression level of ACSL4 in BEAS-2B cells was detected by real-time PCR. The mRNA level of ACSL4 in the siNC+CSE group was significantly increased compared with that in the siNC group, and the mRNA level was significantly decreased in the siACSL4 group. Compared with the siNC+CSE group, the ACSL4 mRNA level in the siACSL4+CSE group was significantly decreased. ACSL4 mRNA expression was significantly elevated in the siACSL4+CSE group compared to the siACSL4 group. The siACSL4+CSE+Fer-1 group showed a significant decrease in ACSL4 mRNA levels compared to the siACSL4+CSE group when given both siACSL4 and Fer-1 (Figure 4A).

The expression levels of ACSL4 and the ferroptosis-related proteins GPX4 and FTH in the cells were detected by Western blotting. Compared with the siNC group, the siNC+CSE group showed significantly increased protein expression of ACSL4 and significantly decreased protein expression of GPX4 and FTH, while the siACSL4 group showed a significant decrease in ACSL4 protein expression and significant increases in the protein expression levels of GPX4 and FTH. The siACSL4+CSE group showed significantly decreased protein expression of ACSL4 and significantly increased expression levels of GPX4 and FTH compared to the siNC+CSE group. Compared to the siACSL4 group, the siACSL4+CSE group showed significantly increased expression of ACSL4 protein and decreased protein expression levels of GPX4 and FTH. Compared to the siACSL4+CSE group, the siACSL4+CSE+Fer-1 group showed a significant decrease in ACSL4 protein expression and significant increases in GPX4 and FTH protein expression levels (Figure 4B).

CCK-8 was used to detect cell viability in each group. The cell viability of the siNC+CSE group was significantly decreased compared to that of the siNC group, and the cell viability of the siACSL4 group was not markedly increased. In comparison to the siNC+CSE group, the cell viability of the siACSL4+CSE group was significantly increased.

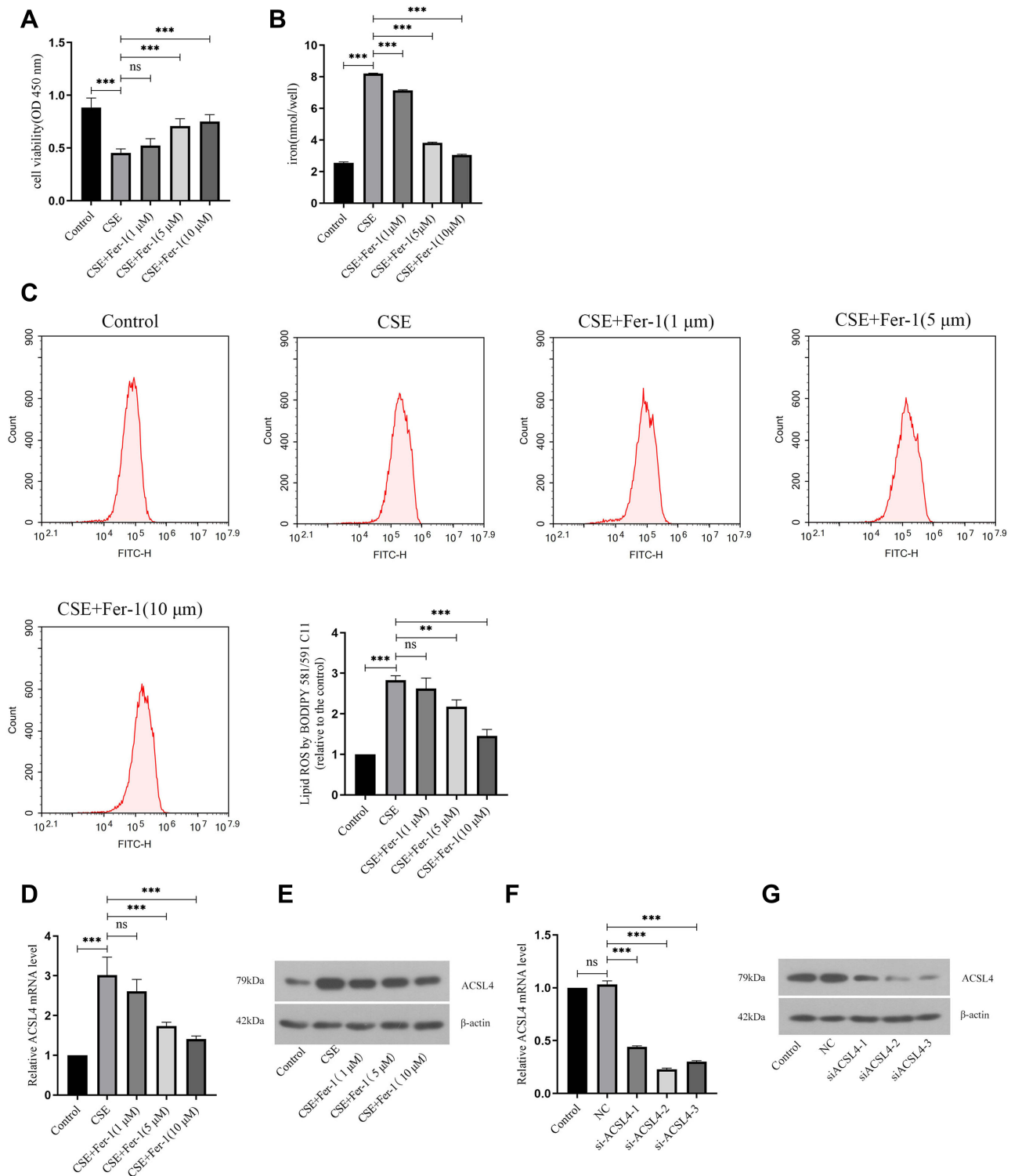


**Figure 3** ACSL4 induces ferroptosis in COPD lung epithelial cells. **(A)** CCK-8 determination of cell viability in each group. **(B)** Detection of iron ion content in cells of each group. **(C)** Lipid ROS content of cells in each group. **(D)** Relative expression levels of ACSL4 mRNA in each cell group. **(E)** ACSL4 protein expression in cells of each group. **(F and G)** Three siRNAs against human ACSL4 and control NC were constructed and transferred into BEAS-2B cells using transfection reagents. Real-time PCR and Western blotting were used to detect the ACSL4 mRNA and protein expression in the cells, respectively, and the siRNAs with the best interference efficiency were screened. Data are presented as the mean ± SD of three replicates and analyzed using one-way ANOVA followed by post-hoc multiple comparisons. (<sup>ns</sup>p > 0.05, <sup>\*\*</sup>p < 0.01, <sup>\*\*\*</sup>p < 0.001).

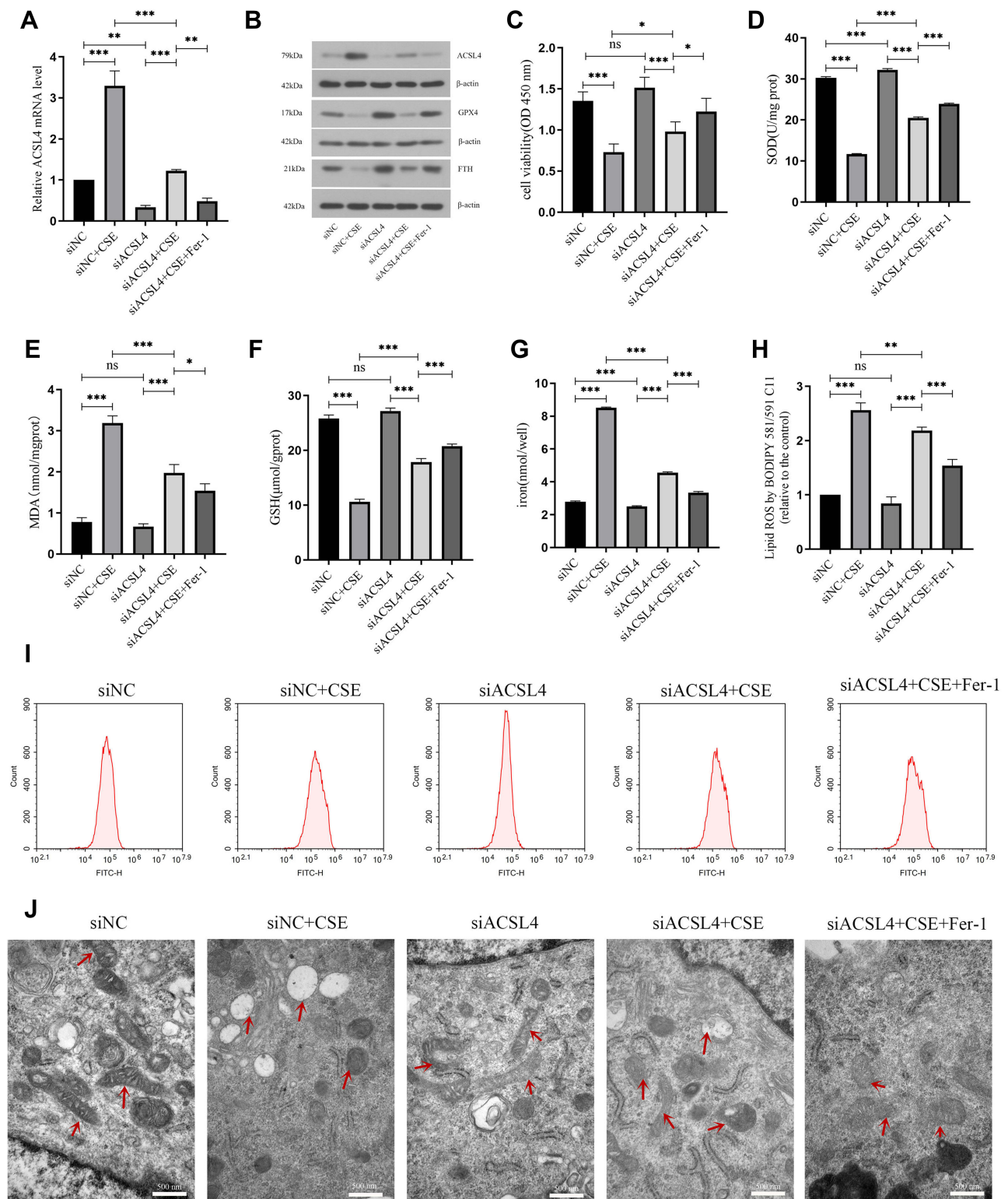


**Figure 4** Interference with ACSL4 can alleviate ferroptosis in lung epithelial cells. **(A)** Relative expression level of ACSL4 mRNA in each group of cells after siRNA interference. **(B)** ACSL4, GPX4 and FTH protein expression in each group after siRNA interference. **(C)** CCK-8 detection of cell viability in each group. **(D–F)** Content detection of the ferroptosis related markers SOD, MDA and GSH. **(G)** Detection of iron ion content in cells of each group. **(H and I)** Detection of lipid ROS content by the BODIPY 581/591 C11 probe method. **(J)** Observation of mitochondrial morphology in cells of each group by transmission electron microscopy. Red arrows indicate mitochondria. Data are presented as the mean  $\pm$  SD of three replicates and analyzed using one-way ANOVA followed by post-hoc multiple comparisons. ( $^{*}p > 0.05$ ,  $^{*}p < 0.05$ ,  $^{**}p < 0.01$ ,  $^{***}p < 0.001$ ).

Compared with the siACSL4 group, the cell viability of the siACSL4+CSE group was significantly decreased. Compared with the siACSL4+CSE group, the cell viability of the siACSL4+CSE+Fer-1 group was significantly increased (Figure 4C).

To further verify the effect of interfering with ACSL4 on ferroptosis in lung epithelial cells, this study conducted an experimental assay related to ferroptosis. First, ferroptosis-related markers were detected. Compared to the siNC group, the siNC+CSE group had significantly lower SOD and GSH levels and significantly higher MDA levels. SOD levels in the siACSL4 group were significantly higher than those in the siNC group, but the GSH and MDA levels were not significantly different. Compared to the siNC+CSE group, the siACSL4+CSE group had significantly higher SOD and GSH levels and significantly lower MDA levels. Compared with the siACSL4 group, the siACSL4+CSE group had significantly lower SOD and GSH levels and significantly higher MDA levels. Compared to the siACSL4+CSE group, the siACSL4+CSE+Fer-1 group had significantly higher SOD and GSH levels and significantly lower MDA levels (Figure 4D–F).

Subsequently, the deposition of intracellular iron ions was detected. Compared to the siNC group, the siNC+CSE group had significantly higher iron ion content, and the siACSL4 group had significantly lower iron ion content. The iron ion levels were significantly reduced in the siACSL4+CSE group compared to the siNC+CSE group. Iron ion levels were significantly elevated in the siACSL4+CSE group compared to the siACSL4 group, while they were significantly reduced in the siACSL4+CSE+Fer-1 group compared to the siACSL4+CSE group (Figure 4G).

Next, the lipid ROS content was detected by flow cytometry. Compared to the siNC group, the siNC+CSE group had significantly higher lipid ROS content, while the siACSL4 group had no significant difference. Compared to the siNC+CSE group, the siACSL4+CSE group had significantly lower lipid ROS content. Compared to the siACSL4 group, the siACSL4+CSE group had significantly higher lipid ROS content. Compared to the siACSL4+CSE group, siACSL4+CSE+Fer-1 lipid ROS levels were significantly reduced (Figure 4H–I).

Finally, morphological changes in mitochondria in lung epithelial cells were observed by transmission electron microscopy. Most mitochondria in siNC cells were morphologically intact, double membrane-coated with clearly visible cristae. In siNC+CSE, the mitochondrial morphology changed, shrinkage and severe vacuolization were observed, and the cristae disappeared. Shrunken mitochondria were present in siACSL4, but most of the mitochondria had normal morphology with clearly visible cristae. In the siACSL4+CSE and siACSL4+CSE+Fer-1 groups, some mitochondrial morphology was restored, with double membranes and cristae visible, but some vacuolated mitochondria still existed (Figure 4J).

## Discussion

Ferroptosis is a novel form of iron-dependent, nonapoptotic cell death caused by excessive accumulation of iron-dependent reactive oxygen species (ROS) and lipid peroxides.<sup>14</sup> Previous studies have shown that ferroptosis is involved in pathophysiologic processes in a variety of diseases.<sup>15–18</sup> Increasing studies have reported that ferroptosis is also involved in the development of respiratory diseases. Zhou et al used oleic acid to induce a mouse model of Acute lung injury (ALI), lung cell mitochondria atrophy, mitochondrial membrane rupture, iron overload, glutathione depletion, and MDA accumulation, suggesting that ferroptosis participates in ALI pathogenesis.<sup>19</sup> Ferroptosis was found in lung tissue from both patients with pulmonary fibrosis and mice with pulmonary disease.<sup>20</sup> Although cigarette smoking is the most important risk factor for COPD, studies have revealed that iron and ferroptosis play a critical role in the development of COPD induced by cigarette smoke, but the precise mechanism remains unknown. One study analysed alveolar irrigation lotions in rats exposed to cigarette smoke as well as smoking COPD patients and found that particulate cigarette smoke may alter iron homeostasis, trigger metal accumulation, affect oxidative stress and inflammation, and lead to lung damage in smoking COPD patients.<sup>21</sup> The results of this study revealed that ACSL4 can mediate ferroptosis in lung epithelial cells and participate in COPD occurrence.

With ferroptosis, intracellular iron storage decreases,  $\text{Fe}^{2+}$  increases and excess  $\text{Fe}^{2+}$  catalyses the Fenton reaction, producing large amounts of ROS and hydroxyl radicals as well as other oxidizing substances that may combine with polyunsaturated fatty acids to form a large quantity of lipid peroxides. Iron chelators such as the ferroptosis inhibitor Fer-1 can reduce iron and lipid peroxidation and thus inhibit ferroptosis.<sup>19,22</sup> SOD is a superoxide dismutase with antioxidant

activity and prevents reactive reactions induced by oxygen species.<sup>23,24</sup> GPX4 is an important antioxidant; GSH is its cofactor, and GSH and GPX4 levels decrease upon ferroptosis.<sup>4,25</sup> Since FTH is an important part of ferritin, which can regulate iron ion storage, decreased FTH expression can increase the free iron level and cause the Fenton reaction to promote ferroptosis.<sup>26,27</sup> These results showed that in the lung tissue of CSE-treated COPD mice and CSE-treated BEAS-2B cells, significant iron deposition occurred, lipid ROS content was increased, SOD and GSH contents were decreased, MDA content was enhanced, and mitochondrial morphogenesis was characterized by ferroptosis. These characteristic changes, mitochondrial shrinkage, vacuolation, and disappearance of cristae demonstrate that ferroptosis occurs in CSE-induced COPD.

There are five subtypes of the ACSL family (ACSL1, ACSL3, ACSL4, ACSL5, and ACSL6), which play their respective functions in fatty acid metabolism. Among them, ACSL4 is not only a sensitive regulator of ferroptosis but also a major contributor to ferroptosis. In general, ACSL4 mediates ferroptosis by carboxylating polyunsaturated fatty acids (PUFAs), followed by the insertion of lysophosphatidylcholine acyltransferase 3 (LPCAT3) into lysophospholipids.<sup>28,29</sup> Upregulation of ACSL4 is a hallmark of ferroptosis.<sup>6</sup> In this study, we found that the protein and mRNA expression levels of ACSL4 in the lung tissue of CSE-induced COPD mice and CSE-treated BEAS-2B cells were significantly upregulated. Following Fer-1 intervention, the levels were significantly reduced, indicating that ACSL4 was highly expressed in lung tissue and lung epithelial cells and was inhibited by Fer-1.

Many studies have demonstrated a promoting effect of ACSL4 on ferroptosis. Knockout of ACSL4 significantly reduces ferroptosis, which in turn inhibits functional and pathological damage in mice with acute kidney injury (AKI).<sup>30</sup> ACSL4 knockdown improves tumour survival/invasiveness and inhibits ferroptosis, whereas ACSL4 overexpression does the opposite *in vivo*.<sup>31</sup> In this experiment, COPD mice were treated with ACSL4-interfering lentivirus (LV-shACSL4), and siRNA was constructed to target ACSL4 in BEAS-2B cells. The results showed that compared with the negative control group, the mRNA and protein expression levels of ACSL4 in cells and animal tissues were significantly upregulated after CSE treatment, while ACSL4 protein and mRNA expression levels were significantly reduced in LV-shACSL4-treated COPD mice and siACSL4 cells. In lung tissues and cells in which ACSL4 expression was not inhibited, iron deposition was evident, lipid peroxidation occurred, ferroptosis-related indices were altered, and mitochondrial morphology was characterized. These results suggest that ACSL4 contributes to ferroptosis in CSE-induced COPD mice model and CSE-stimulated epithelial cells, that interference with ACSL4 inhibits ferroptosis in COPD mice model, and that ACSL4 expression levels are positively associated with CSE-mediated ferroptosis in epithelial cells.

## Conclusion

ACSL4-mediated ferroptosis in lung epithelial cells is associated with COPD and positively correlated with ferroptosis in epithelial cells.

## Ethics Approval

The animal experiments involved in this study were approved by the Ethical Committee of Central Hospital Affiliated to Shenyang Medical College (2020 [0008]). The animals used in the study were maintained according to Guide for the Care and Use of Laboratory Animals of the National Institutes of Health. Humane care is provided in accordance with the 3R principles of animal testing.

## Funding

This work was supported by Key R&D Program Guidance Projects in Liaoning Province (2019JH8/10300051), National Natural Science Foundation of China (82072008).

## Disclosure

The authors declare no competing interests in this work.

## References

1. Nguyen JMK, Robinson DN, Sidhaye VK. Why new biology must be uncovered to advance therapeutic strategies for chronic obstructive pulmonary disease. *Am J Physiol Lung Cell Mol Physiol*. 2021;320(1):L1–L11. doi:10.1152/ajplung.00367.2020
2. Sheikh K, Coxson HO, Parraga G. This is what COPD looks like. *Respirology*. 2016;21(2):224–236. doi:10.1111/resp.12611
3. Sadeghi L, Yousefi Babadi V, Espanani HR. Toxic effects of the Fe<sub>2</sub>O<sub>3</sub> nanoparticles on the liver and lung tissue. *Bratisl Lek Listy*. 2015;116(6):373–378. doi:10.4149/bl\_2015\_071
4. Dixon SJ, Lemberg KM, Lamprecht MR, et al. Ferroptosis: an iron-dependent form of nonapoptotic cell death. *Cell*. 2012;149(5):1060–1072. doi:10.1016/j.cell.2012.03.042
5. Yoshida M, Minagawa S, Araya J, et al. Involvement of cigarette smoke-induced epithelial cell ferroptosis in COPD pathogenesis. *Nat Commun*. 2019;10(1):3145. doi:10.1038/s41467-019-10991-7
6. Yuan H, Li X, Zhang X, Kang R, Tang D. Identification of ACSL4 as a biomarker and contributor of ferroptosis. *Biochem Biophys Res Commun*. 2016;478(3):1338–1343. doi:10.1016/j.bbrc.2016.08.124
7. Doll S, Proneth B, Tyurina YY, et al. ACSL4 dictates ferroptosis sensitivity by shaping cellular lipid composition. *Nat Chem Biol*. 2017;13(1):91–98. doi:10.1038/nchembio.2239
8. Wang Y, Bi R, Quan F, et al. Ferroptosis involves in renal tubular cell death in diabetic nephropathy. *Eur J Pharmacol*. 2020;888:173574. doi:10.1016/j.ejphar.2020.173574
9. Xu Y, Li X, Cheng Y, Yang M, Wang R. Inhibition of ACSL4 attenuates ferroptotic damage after pulmonary ischemia-reperfusion. *FASEB J*. 2020;34(12):16262–16275. doi:10.1096/fj.202001758R
10. Zhu ZY, Liu YD, Gong Y, et al. Mitochondrial aldehyde dehydrogenase (ALDH2) rescues cardiac contractile dysfunction in an APP/PS1 murine model of Alzheimer's disease via inhibition of ACSL4-dependent ferroptosis. *Acta Pharmacol Sin*. 2022;43(1):39–49. doi:10.1038/s41401-021-00635-2
11. Xing YH, Zhang JL, Lu L, et al. Identification of specific gene modules in mouse lung tissue exposed to cigarette smoke. *Asian Pac J Cancer Prev*. 2015;16(10):4251–4256. doi:10.7314/apjcp.2015.16.10.4251
12. He X, Li T, Luo L, Zeng H, Chen Y, Cai S. PRMT6 mediates inflammation via activation of the NF-kappaB/p65 pathway on a cigarette smoke extract-induced murine emphysema model. *Tob Induc Dis*. 2020;18:8. doi:10.18332/tid/116413
13. Zhang Z, Fu C, Liu J, et al. Hypermethylation of the Nrf2 promoter induces ferroptosis by inhibiting the Nrf2-GPX4 axis in COPD. *Int J Chron Obstruct Pulmon Dis*. 2021;16:3347–3362. doi:10.2147/COPD.S340113
14. Chen X, Li J, Kang R, Klionsky DJ, Tang D. Ferroptosis: machinery and regulation. *Autophagy*. 2021;17(9):2054–2081. doi:10.1080/15548627.2020.1810918
15. Mahoney-Sanchez L, Bouchaoui H, Ayton S, Devos D, Duce JA, Devedjian JC. Ferroptosis and its potential role in the pathophysiology of Parkinson's Disease. *Prog Neurobiol*. 2021;196:101890. doi:10.1016/j.pneurobio.2020.101890
16. Wang Y, Kuang X, Yin Y, et al. Tongxinluo prevents chronic obstructive pulmonary disease complicated with atherosclerosis by inhibiting ferroptosis and protecting against pulmonary microvascular barrier dysfunction. *Biomed Pharmacother*. 2022;145:112367. doi:10.1016/j.biopha.2021.112367
17. Li D, Jiang C, Mei G, et al. Quercetin alleviates ferroptosis of pancreatic beta cells in type 2 diabetes. *Nutrients*. 2020;12(10). doi:10.3390/nu12102954
18. Tao W, Liu F, Zhang J, Fu S, Zhan H, Qian K. miR-3587 inhibitor attenuates ferroptosis following renal ischemia-reperfusion through HO-1. *Front Mol Biosci*. 2021;8:789927. doi:10.3389/fmolb.2021.789927
19. Zhou H, Li F, Niu JY, et al. Ferroptosis was involved in the oleic acid-induced acute lung injury in mice. *Sheng Li Xue Bao*. 2019;71(5):689–697. doi:10.13294/j.aps.2019.0070
20. Lin Z, Xu Y, Guan L, et al. Seven ferroptosis-specific expressed genes are considered as potential biomarkers for the diagnosis and treatment of cigarette smoke-induced chronic obstructive pulmonary disease. *Ann Transl Med*. 2022;10(6):331. doi:10.21037/atm-22-1009
21. Ghio AJ, Hilborn ED, Stonehuerner JG, et al. Particulate matter in cigarette smoke alters iron homeostasis to produce a biological effect. *Am J Respir Crit Care Med*. 2008;178(11):1130–1138. doi:10.1164/rccm.200802-334OC
22. Wen X, Wu J, Wang F, Liu B, Huang C, Wei Y. Deconvoluting the role of reactive oxygen species and autophagy in human diseases. *Free Radic Biol Med*. 2013;65:402–410. doi:10.1016/j.freeradbiomed.2013.07.013
23. Barrera G. Oxidative stress and lipid peroxidation products in cancer progression and therapy. *ISRN Oncol*. 2012;2012:137289. doi:10.5402/2012/137289
24. Sun WH, Liu F, Chen Y, Zhu YC. Hydrogen sulfide decreases the levels of ROS by inhibiting mitochondrial complex IV and increasing SOD activities in cardiomyocytes under ischemia/reperfusion. *Biochem Biophys Res Commun*. 2012;421(2):164–169. doi:10.1016/j.bbrc.2012.03.121
25. Krummel B, Plotz T, Jorns A, Lenzen S, Mehmeti I. The central role of glutathione peroxidase 4 in the regulation of ferroptosis and its implications for pro-inflammatory cytokine-mediated beta-cell death. *Biochim Biophys Acta Mol Basis Dis*. 2021;1867(6):166114. doi:10.1016/j.bbdis.2021.166114
26. Blankenhaus B, Braza F, Martins R, et al. Ferritin regulates organismal energy balance and thermogenesis. *Mol Metab*. 2019;24:64–79. doi:10.1016/j.molmet.2019.03.008
27. Lu R, Jiang Y, Lai X, Liu S, Sun L, Zhou ZW. A shortage of FTH Induces ROS and sensitizes RAS-proficient neuroblastoma N2A cells to ferroptosis. *Int J Mol Sci*. 2021;22(16):8898. doi:10.3390/ijms22168898
28. Jiang X, Stockwell BR, Conrad M. Ferroptosis: mechanisms, biology and role in disease. *Nat Rev Mol Cell Biol*. 2021;22(4):266–282. doi:10.1038/s41580-020-00324-8
29. Chen X, Kang R, Tang D. Ferroptosis by lipid peroxidation: the tip of the iceberg? *Front Cell Dev Biol*. 2021;9:646890. doi:10.3389/fcell.2021.646890
30. Wang Y, Zhang M, Bi R, et al. ACSL4 deficiency confers protection against ferroptosis-mediated acute kidney injury. *Redox Biol*. 2022;51:102262. doi:10.1016/j.redox.2022.102262
31. Zhang Y, Li S, Li F, Lv C, Yang QK. High-fat diet impairs ferroptosis and promotes cancer invasiveness via downregulating tumor suppressor ACSL4 in lung adenocarcinoma. *Biol Direct*. 2021;16(1):10. doi:10.1186/s13062-021-00294-7

International Journal of Chronic Obstructive Pulmonary Disease

Dovepress

### Publish your work in this journal

The International Journal of COPD is an international, peer-reviewed journal of therapeutics and pharmacology focusing on concise rapid reporting of clinical studies and reviews in COPD. Special focus is given to the pathophysiological processes underlying the disease, intervention programs, patient focused education, and self management protocols. This journal is indexed on PubMed Central, MedLine and CAS. The manuscript management system is completely online and includes a very quick and fair peer-review system, which is all easy to use. Visit <http://www.dovepress.com/testimonials.php> to read real quotes from published authors.

Submit your manuscript here: <https://www.dovepress.com/international-journal-of-chronic-obstructive-pulmonary-disease-journal>